

# FRAP analysis

## Measuring biophysical kinetic parameters using image analysis

Sharva V Hiremath\* Gregory Reeves† Cranos M. Williams\*

\*Department of Electrical and Computer Engineering, North Carolina State University, Raleigh, U.S.

†Department of Chemical Engineering, Texas AM University, Austin, U.S.

**Abstract**—Understanding transcription factor dynamics is crucial for unraveling the regulatory mechanisms of gene expression that underpin cellular function and development. Measurements of transcription factor subcellular movement are essential for developing predictive models of gene expression. However, obtaining these quantitative measurements poses significant challenges due to the inherent variability of biological data and the need for high precision in tracking the movement and interaction of molecules. Our computational pipeline provides a critical solution to these challenges, offering a comprehensive approach to the quantitative analysis of transcription factor dynamics. By integrating advanced image segmentation to accurately delineate individual nuclei, precise nucleus tracking to monitor changes over time, and detailed intensity extraction to measure fluorescence as a proxy for transcription factor activity, our pipeline enables the estimation of vital biophysical parameters.

**Index Terms**—nuclei segmentation, nuclei tracking, confocal microscopy, FRAP, *Drosophila Melanogaster*

### I. INTRODUCTION

Regulation of gene expression is critical across all areas of biology, often mediated by transcription factors that enter the nucleus to bind to specific DNA sequences, thereby controlling gene activation or repression. For a comprehensive understanding of the relationship between transcription factor dynamics and gene expression, it is imperative to quantitatively analyze transcription factor movements within cells [1]–[4]. Specifically, insights into the rates of nuclear import and export of transcription factors are vital, as they elucidate how variations in the bulk concentration of transcription factors within the nucleus can influence gene expression decisions, thereby affecting cellular function and organismal development [5]–[8].

In this context, our paper leverages these insights to quantify the nuclear import and export rates of the transcription factor Dorsal (Dl), which exhibits a spatial gradient of nuclear concentration in 1-3 hour old *Drosophila melanogaster* embryos [9]. We elucidate the methodology of our image analysis protocol and detail the computational steps involved in data fitting. Our approach effectively extracts biophysical parameters related to Dorsal, demonstrating the efficacy of our pipeline.

Fluorescence Recovery After Photobleaching (FRAP) assays are a critical tool for quantifying protein movement. Introduced in the 1970s primarily to observe the mobility of fluorescently tagged molecules on cell surfaces [10], FRAP assays have evolved significantly with the advent of Green

Fluorescent Protein (GFP) technology. This evolution has broadened their application in exploring protein behaviors within cells [11], [12].

FRAP assays provide a distinctive perspective on protein dynamics. By intentionally bleaching a specific area in a cell or tissue and observing how fluorescence returns, researchers can extract valuable information about protein movement, interaction, and turnover rates [13]–[16]. The strength of FRAP assays lies not just in their capacity to yield quantitative data, but also in their suitability for live cell and tissue studies, rendering them crucial for investigating protein dynamics. However, in order to be able to extract measurements from the fluorescent image data, an image analysis pipeline is necessary.

To overcome the challenges associated with data variability and the requirement for attributes such as intensity or shape to remain consistent across different locations and time frames, we have developed a new computational pipeline. This pipeline skillfully merges FRAP assays with advanced image analysis techniques to derive quantitative measurements. Unlike the numerous existing methods proposed for locating/segmenting nuclei and tracking them [17]–[27], which we have dismissed due to these challenges, our approach is designed to be more adaptable and reliable under varying conditions. It involves three key steps: image segmentation, nucleus tracking, and intensity extraction, all of which contribute to the subsequent data fitting step for parameter extraction. Here, we propose a computational pipeline that combines FRAP assays with image analysis techniques to extract quantitative measurements.

The image analysis pipeline consists of three major steps: (1) image segmentation, to accurately delineate individual nuclei from the surrounding biological milieu; (2) nucleus tracking, to monitor the movement and changes in position of each nucleus over time; and (3) intensity extraction, to measure the fluorescence intensity as a proxy for various biological phenomena. Each of these steps are designed to ensure the integrity of the data is preserved, facilitating a seamless transition to the data fitting phase. Here, the extracted parameters serve as the foundation for in-depth analysis and interpretation. By integrating these components into a cohesive pipeline, we not only streamline the process of data analysis but also enhance the reliability and accuracy of the results obtained. This pipeline is particularly advantageous in scenarios where traditional methods prove inadequate due to the intricate nature

of the data or the specific demands of the research question at hand. Through the application of our pipeline, researchers are equipped to navigate the complexities of biological data, enabling a deeper understanding of the underlying mechanisms at play.

## II. MATERIALS AND METHODS

### A. Data collection

The data collected for measuring the import/export rates uses two fluorescent proteins (FPs) captured across two channels, which collect structural information and protein signal data.

The first channel (the nuclear channel), consists of the structural information where the nuclei are highlighted by staining them with Histone, which is a red fluorescent protein (RFP). The second channel (the nuclear protein channel), is one where we actually observe the change in intensity of the bleached nucleus by tagging the gene of interest, which in this case is DI, with a green fluorescent protein (GFP). The data are collected from two locations of the embryo (dorsal and ventral), each looking at the behavior of protein at different locations along the DV-axis. (Fig. 2).

We use the nuclear channel to locate/segment the nuclei. Next, we map this location information on the protein channel to obtain intensity measurements of the bleached nucleus. Finally, these values are fitted to calculate the import/export rates.

GFP, fused to DI (DI-GFP) [7], is bleached using a high-power laser in a single nucleus, and the recovery of nuclear fluorescence, achieved by the movement of cytoplasmic DI-GFP molecules into the bleached nucleus to replenish the bleached-out nucleus, is measured. This recovery quantifies the rate at which the protein (by proxy of relative intensity) moves in and out of the nucleus (Fig. 2).

### B. Challenges with image data

The methodology for analyzing microscopy images is intricately linked to the complexities of the data obtained from experimental processes. These challenges, which significantly influence the analysis approach, are multifaceted and cover various issues related to the dynamic and variable characteristics of the observed specimens.

One primary challenge involves intensity variation, where the brightness of individual nuclei changes over time, coupled with differences in intensity observed among nuclei within the same time frame. This variability complicates the consistent observation and analysis of these nuclei.

In addition to changes in internal structure, the shape of nuclei can vary over time and across different nuclei within a single observation period. These shape changes, characterized by unique and irregular contours, pose additional challenges in tracking and analyzing each nucleus accurately. The proximity of nuclei to one another further complicates this task, as it becomes challenging to distinguish between closely situated nuclei, to ascertain individual identities.

High levels of movement among the nuclei introduce further difficulties in tracking and maintaining consistent identification. This is particularly problematic when nuclei exhibit rapid or extensive motion, which can lead to errors in tracking continuity. Lastly, the issue of target re-identification emerges when nuclei move in and out of the observational frame, complicating the task of keeping consistent labels on them throughout the study period. These challenges collectively demand analytical approaches and methodologies to accurately interpret microscopy images and derive meaningful insights from experimental data.

### C. Proposed approach overview

The analysis of microscopy data collected from FRAP experiments can broadly be classified into two parts, namely image analysis and data fitting. Image Analysis consists of locating the nuclei, tracking the bleached nucleus and surrounding nuclei, and extracting the intensity of nuclei from the protein channel. Data fitting consists of empirically fitting these intensities to a function to obtain the import/export rates (Fig. 3).

Tracking the bleached nucleus through the different time frames is essential as we need to measure how the fluorescence recovers over time in the bleached nucleus. In addition, due to unintentional bleaching, in which the regular acquisition of data slowly bleaches all GFP molecules in the frame, it is equally important to track the other surrounding nuclei as well. If the intensity of the surrounding nuclei decreases over time, it can be attributed to unintentional bleaching. We use these measurements to normalize the recovery of the intentionally bleached nucleus (see Extracting intensities of nuclei and cytoplasm).

For analyzing FRAP images and solving the challenges associated with it, we decided to use Watershed for segmentation. It allows us to deal with local issues individually instead of resorting to a global-based solution. This approach suits us well as it simultaneously addresses the variations in intensity, shape, and overlapping nuclei.

After segmenting the nuclei, we initiate the tracking process. Our approach is influenced by several constraints, including the potential for high movement (due to data being collected close to gastrulation) and the movement of nuclei in and out of the frame. These factors introduce complexities in simultaneously tracking multiple nuclei across frames exhibiting changing intensity profiles, evolving shapes, and nuclei entering or exiting the frame. In response to these challenges, we employ a Point registration approach [29]–[32]. This method allows for the simultaneous tracking of multiple objects, obviating the need to search each frame for matching objects in a sequential manner, which increases the overall complexity.

### D. Segmentation

Before segmentation, we perform pre-processing to prepare the data for segmentation. First, we correct image defects caused by uneven illumination in fluorescent microscopy using background correction by multiplying the image data (array) with a scalar value. This step helps improve the illumination

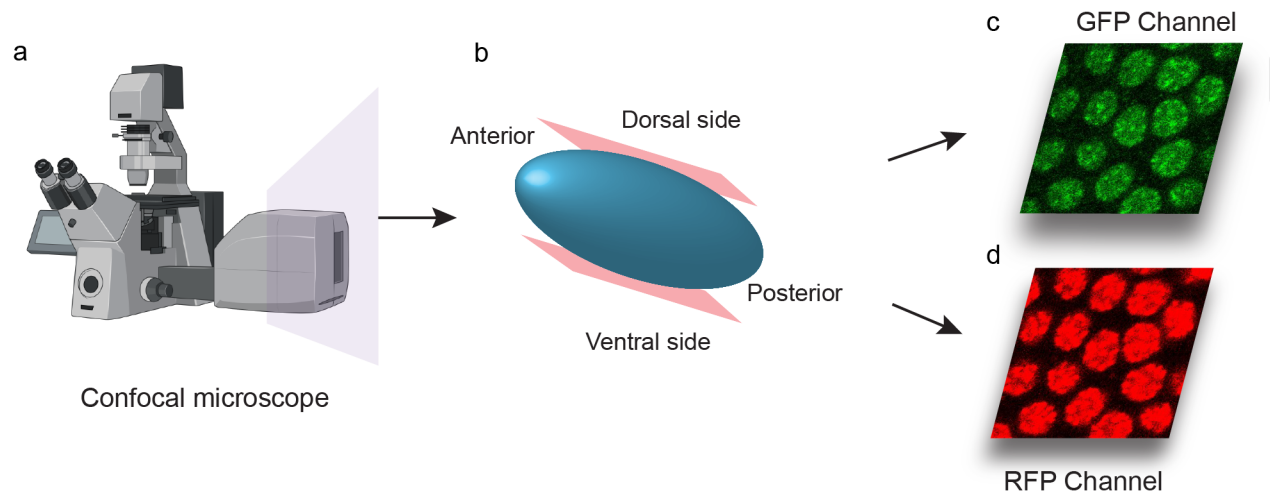


Fig. 1. FRAP experiment setup and data collection. (a) Illustration of the setup for collecting the image data from FRAP experiments using a confocal microscope (Created with BioRender.com). (b) The data is collected from 2 cross sections of the embryo, i.e., the dorsal and ventral side, for measuring import/export rates. (c,d) Image data collected for 2 channels.

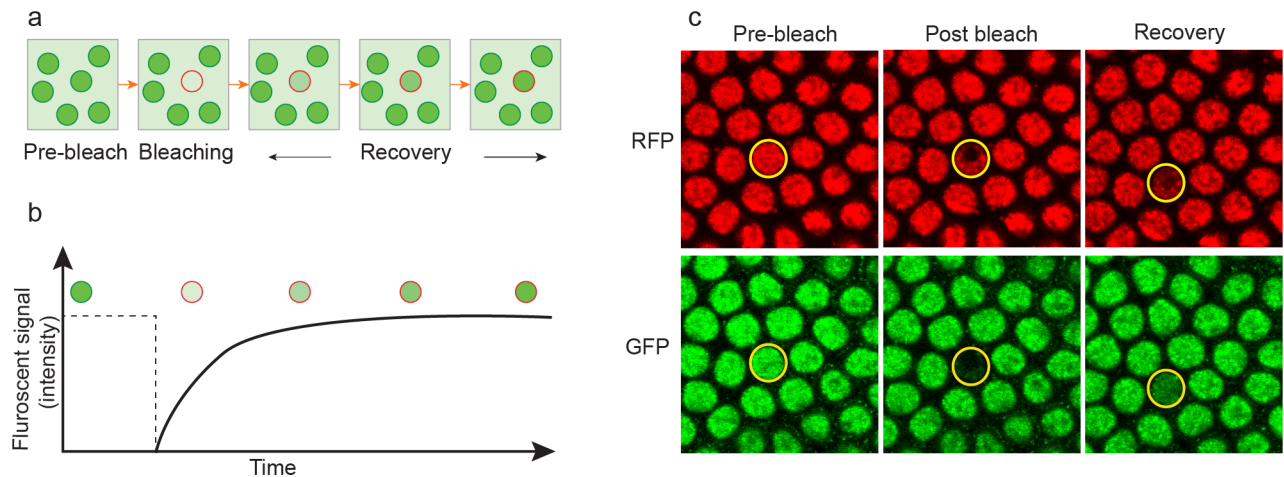


Fig. 2. (a) In FRAP assays, the time that fluorescent molecules need to replenish a bleached-out area is measured, basically assessing how quickly a dark sample area turns bright again [28]. We photobleach one nucleus using a high-power laser pulse to alter the fluorophore molecules attached to the protein, such that they are unable to fluoresce. (b) Illustration of the recovery of fluorescence observed in the bleached nucleus over time. The bleached nucleus (highlighted by red circle) undergoes an exchange of protein tagged with FP's from the surrounding cytoplasm. This exchange with the surrounding cytoplasm leads to the eventual recovery in intensity observed. (c) Here we have an example of what the data looks like. The bleached nucleus is indicated by the circle in yellow. We can observe how the intensity of the bleached nucleus disappears initially after bleaching before reappearing later in GFP but remains visible throughout in RFP.

of both nuclei and cytoplasm, making them sufficiently visible to be accurately identified during the segmentation process. Then, we use gaussian blurring to smoothen the disparities in intensity within nuclei caused by an accumulation of fluorophores (FPs) in a few locations. Incorporating Gaussian blurring in the preprocessing phase helps to mitigate the issue of oversegmentation, since it improves the determination and selection of appropriate nuclear and background markers.

Next, we calculate the regional maxima for the images, and these maxima are used as foreground markers for the marker-based watershed. Using the watershed technique allows us to obtain ridge lines (watershed lines) that separate the image into compartments that each contain a single nucleus. This is

effective as we can now split each nucleus into its own territory and process it without affecting the others. Using this approach also alleviates issues where global approaches to segmenting nuclei don't work due to variations in intensity among the nuclei and other local issues. Additionally, we store these ridge lines as they can be used to associate cytoplasmic regions to the various nuclei. We use these to obtain the intensity of cytoplasm around the bleached nucleus and surrounding nuclei in the later stages of the pipeline.

After isolating the individual compartments, we create a set of temporary, empty arrays, ensuring the count of these arrays corresponds exactly to the number of compartments. Each array is created to match the original image size, and

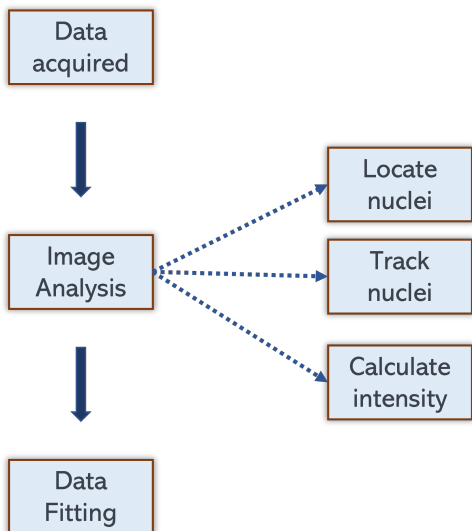


Fig. 3. Broad overview of steps in the pipeline for analysing FRAP images

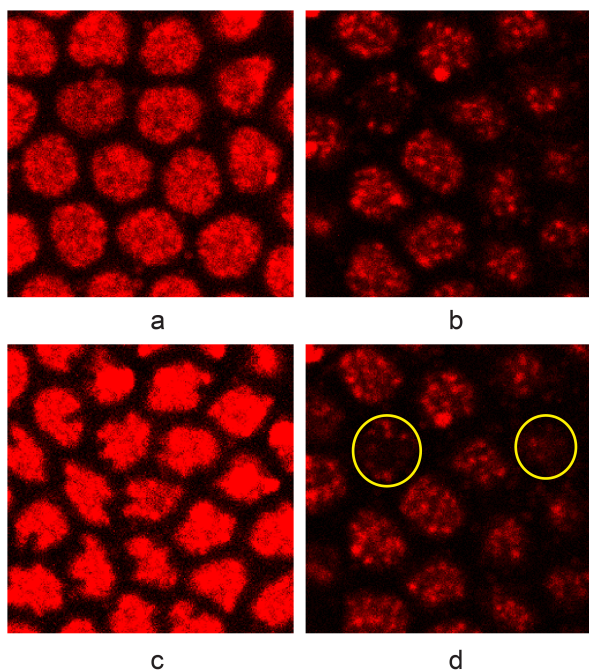


Fig. 4. Challenges in nuclei detection. (A) Idea case for nuclei (B) Variation in intensity within nuclei (C) Irregularly shaped nuclei (D) Nuclei breaking into blobs are encircled

these arrays are populated with the pixel intensities from the nuclear channel that correspond to each specific compartment. Following the transfer of pixel intensities, we apply Otsu’s method [33] for thresholding, which produces a binary mask for each compartment. This approach is effective since we are distinguishing between two primary classes: the nuclei and the cytoplasm. After generating the binary masks for each individual compartment in the temporary arrays, we then stitch together all the binary masks obtained for each compartment containing the nuclei. This merging process yields a unified mask that encompasses all the nuclei across the different compartments.

Once a complete binary mask is determined, it is then cleaned morphologically using erosion followed by dilation with disk-shaped structuring elements of sizes 5 pixels ( $\sim .31 \mu\text{m}$ ) and 1 pixel ( $\sim .062 \mu\text{m}$ ), respectively. This procedure corrects any irregular boundaries and produces a conservative mask, which is particularly useful for the nuclei that might be overlapping. Additionally, we implement a size-based filter to exclude artifacts smaller than 400 pixels. This exclusion criterion is based on the analysis of nuclear size histograms, which indicate an average nuclear radius of approximately 40 pixels ( $\sim 2.5 \mu\text{m}$ ), and an average nuclear area of 5026 pixels. Notably, nuclei that are only partially within the frame exhibit much smaller pixel areas. Removing significantly smaller artifacts prevents the accidental inclusion of cytoplasmic components, ensuring the mask accurately represents nuclear regions only.

This cleaned binary mask is then used to create a nuclear mask that outlines the individual nuclei border. In addition to the nuclear mask, details such as average intensity, pixel locations, and centroid locations are also stored. We can actively utilize these details to analyze the trajectory of nuclei as required.

#### E. Tracking

Once we have the segmented nuclei for each time frame, we track these nuclei. For the first frame, we label the nuclei. In the following frames, we use the locations of the centroids (stored as point clouds) of nuclei detected to identify the nuclei from the previous frames. We identify the nuclei by comparing the constellation of centroids  $C_{t-1}$  from frame  $t-1$  with the constellation of centroids  $C_t$  from frame  $t$  by registering them with each other using an Iterative Closest Point Algorithm [34].

Registering the point clouds gives the transformation matrix which, when applied on  $C_t$ , gives a new set of points  $C'_t$  that best match with  $C_{t-1}$ . Using this, we can infer the identity/label of the nuclei based on which nucleus is closest to it in the transformed coordinates.

In our data set, the nuclei exhibit coordinated motion, forming a constellation. As a result, we can effectively trace the nuclei by relying on their relative positions, thereby addressing the challenge of tracking during periods of significant movement.

To solve the other problem of target re-identification, we add a “lookback feature” in the algorithm. In case there are points in  $C'_t$  that fail to correspond with any points in  $C_{t-1}$ , we can lookback at previous frames to examine if there are any matching points. The number of frames subject to retrospective examination is defined by a user-specified parameter. Consequently, should matching points be identified, the nearest label is assigned, under the presumption of a nucleus reappearing. In the absence of corresponding points, these unmatched points are classified as new nuclei and are accordingly assigned a new label, while ensuring conservation of label number.

##### a) Missing bleached nucleus:

In some instances, following the bleaching event, the bleached

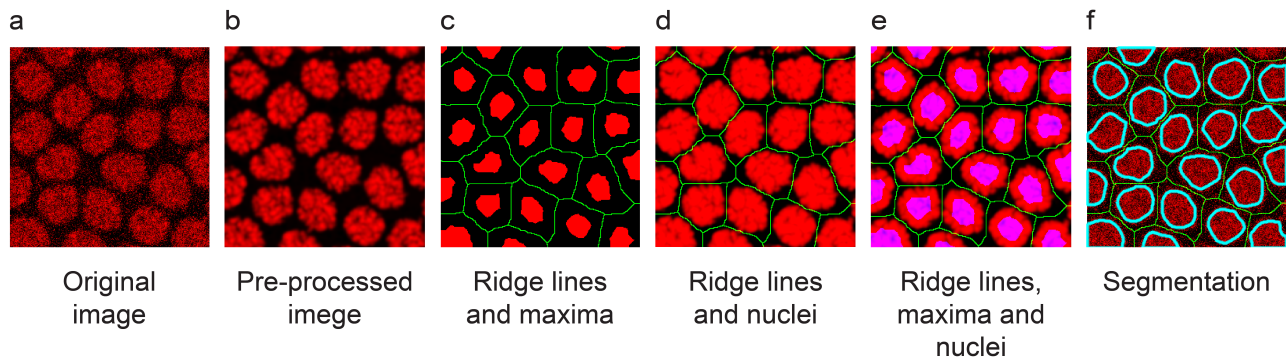


Fig. 5. Different steps of the Image analysis pipeline for FRAP. (A) Raw image data (B) Image after preprocessing using background correction, blurring, and removing small artifacts (C) Regional maxima (in red) and the ridge lines (in green) obtained using watershed (D) Processed data (in red) and ridge lines (in green) (E) Processed data (in red), ridge lines (in green) and regional maxima (in pink) (F) original data, ridge lines (in green) and the nuclear masks obtained using Otsu’s thresholding (in cyan)

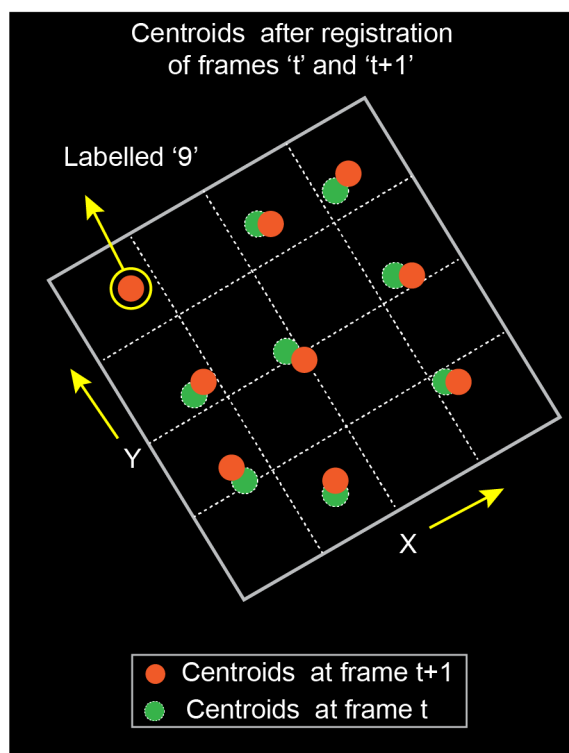


Fig. 6. Example illustrating tracking using Point registration approach. Here we have centroids from frame ‘t’ and the transformed centroids from frame ‘t+1’ juxtaposed on top of each other. We assign labels to the centroids from ‘t+1’ based on analysing the closest centroid from frame ‘t’. If some centroids haven’t appeared previously, we assign them new labels, like the centroid labelled ‘9’, which was not present earlier.

nucleus disappears from both the nuclear and protein channels. To address this scenario, we employ the positional data of neighboring nuclei to trace the whereabouts of the bleached nucleus. Our approach hinges on the assumption that the bleached nucleus maintains its shape throughout the frames during its absence. Leveraging this assumption, we project the nuclear mask of the bleached nucleus across the missing frames by computing the average movement of the adjacent nuclei.

### F. Extracting intensities of nuclei and cytoplasm

We apply the masks derived from segmentation and tracking to the protein channel to calculate the mean intensities. For each nuclear and cytoplasmic compartment, we compute the mean pixel intensity, excluding the lowest and highest five percentiles to mitigate the influence of outliers and noise on the data. This ensures the calculated means accurately reflect the true intensity distribution. Subsequently, we adjust these mean values by subtracting the background intensity.

After extracting the intensities for all the nuclei and cytoplasmic compartments for all the time frames, we examine if any unintentional bleaching has occurred. This issue arises when all the GFP molecules in the frame get bleached over time during data collection. We detect if unintentional bleaching has occurred by looking at the intensities of the neighboring nuclei and cytoplasm. The intensity measurements of the neighboring nuclei and cytoplasm are used to normalize the intensity of the bleached nucleus and its cytoplasmic compartment to accommodate the effects of intentional bleaching. The centroids of the nuclei were utilized to ascertain the proximity of neighboring nuclei. By calculating distances between the bleached nucleus and others, it is possible to identify which nuclei are nearest to the bleached nucleus. A user-defined parameter determines the specific count of nuclei to be regarded as neighbors in this context.

We employ Equation (1) to normalize the intensities of the bleached nucleus and its cytoplasm. Here, ‘ $y_{norm}$ ’ represents the normalized intensity for either the bleached nucleus or cytoplasm, ‘ $y_{blc}$ ’ denotes the intensity of the bleached nucleus or cytoplasm, ‘ $y_{mean}$ ’ indicates the average intensity of surrounding nuclei or cytoplasmic regions, and ‘ $y_{mean}^0$ ’ refers to the initial average intensity of these surrounding areas immediately after the bleaching event.

$$y_{norm} = \frac{y_{blc}}{y_{mean}} * y_{mean}^0 \quad (1)$$

## III. RESULTS AND DISCUSSION

We analyzed FRAP experiments from blastoderm-stage (1-3 h old) *Drosophila* embryos expressing DI-GFP and Histone-RFP (to mark the nuclei) [7]. In these experiments, we took a

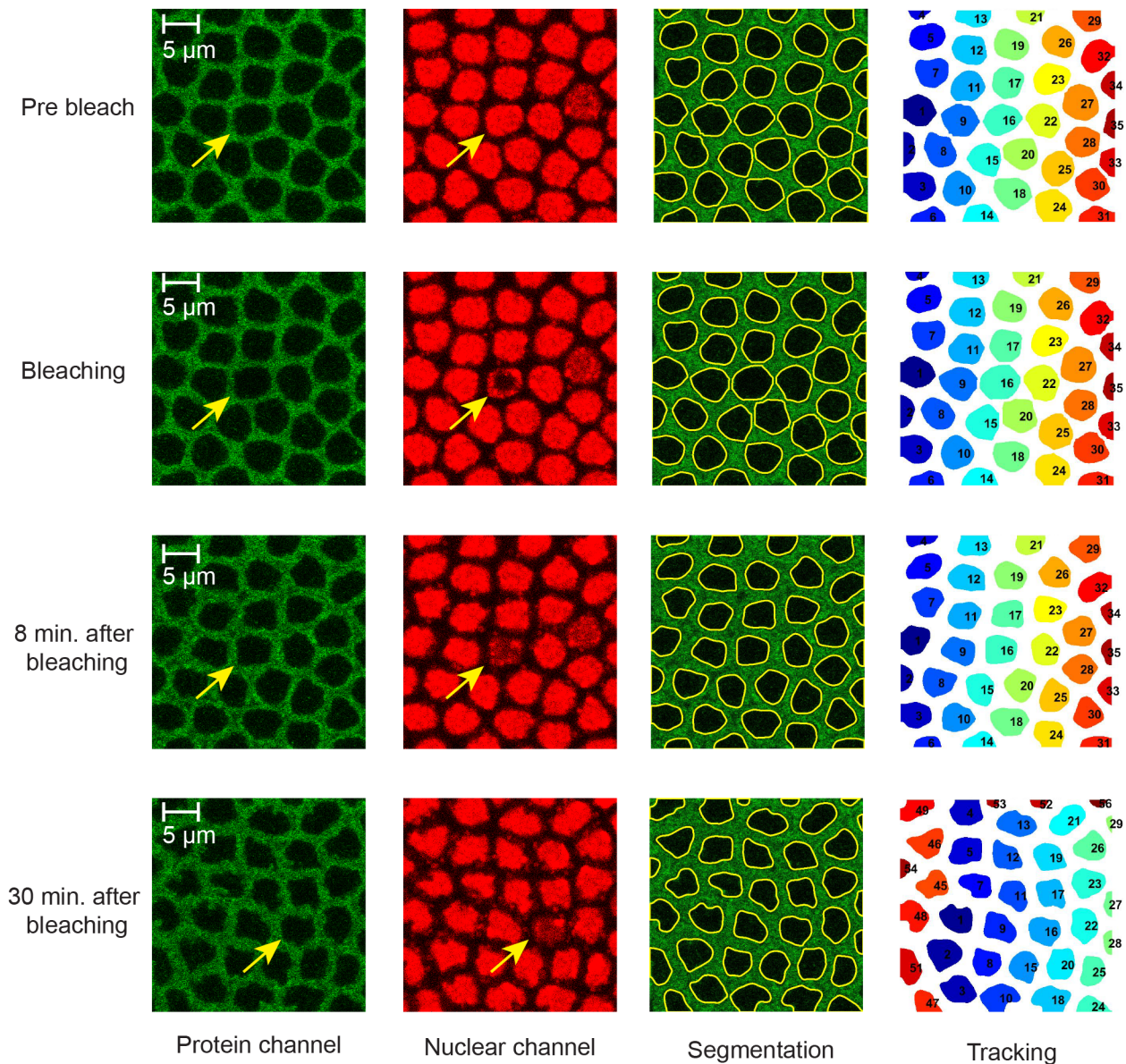


Fig. 7. Results of image analysis when the nuclear int.  $\ll$  cytoplasmic intensity. The bleached nucleus (label number 16) was segmented and tracked through all the time frames along with its neighbors.

snapshot of the region of interest (“Pre-bleach” in Fig. 2c), bleached a single nucleus near the center of the image at time  $t=0$  (“Post bleach” in Fig. 2c), then imaged the nuclei in the region of interest for roughly 15 minutes (“Recovery” in Fig. 2c). To adequately quantify the recovery of the GFP fluorescence in the bleached nucleus, we developed an image analysis pipeline that includes nuclear segmentation (Fig. 5) and nuclear tracking (Fig. 6; see Methods for more details). Using this pipeline, we were able to adequately segment the nuclei in all observed time courses (Figs. 7 and 8). It should be noted that Figs. 7 and 8 present the outcomes for two distinct scenarios: one where the nuclear intensity is significantly lower than that of the cytoplasm and another where the situation is reversed. In both instances, our pipeline demonstrated remarkable adaptability, successfully achieving reliable segmentation

masks and tracking despite the variations.

In our FRAP analysis, the necessity of nucleus tracking, in which we assign to each nucleus a label that persists throughout the time course so that the identity of each nucleus is maintained, cannot be overstated. We used a points registration algorithm in which the centroid coordinates of each nucleus, as found by the nuclear segmentation, are globally correlated between frames (Fig. 6). Thus, the persistence of labels from one frame to the next were the result of an optimization algorithm in which each nucleus was assigned the label to the closest nucleus from the previous frame. Once the nuclei were properly tracked (e.g., Figs. 7 and 8), it allowed us to identify the fluorescence recovery of the bleached nucleus (Fig. 9a). Furthermore, it allowed us to identify the fluorescence time course of the other nuclei in the

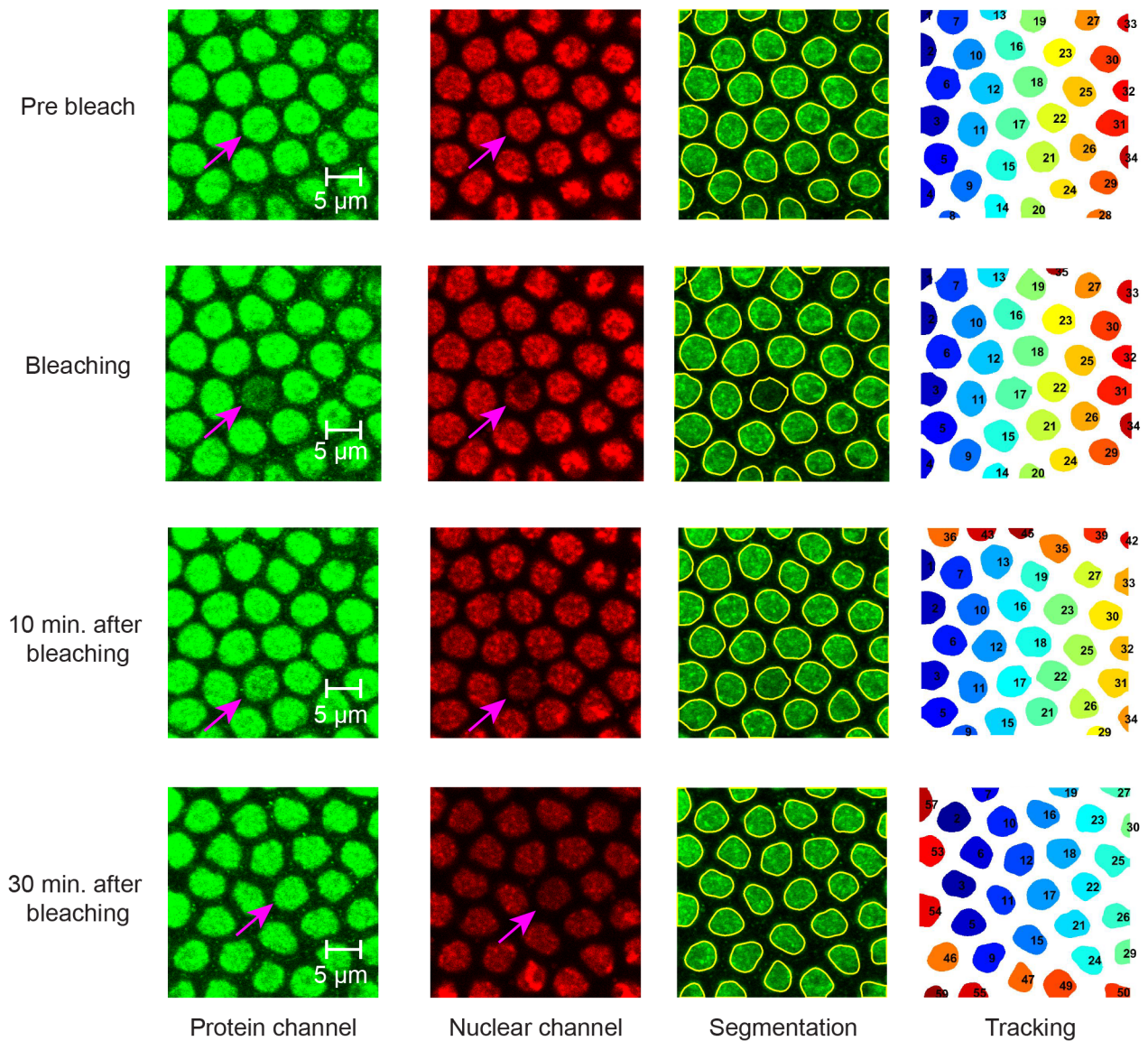


Fig. 8. Results of image analysis when the nuclear int.  $\gg$  cytoplasmic intensity. The bleached nucleus (label number 17) was segmented and tracked through all the time frames along with its neighbors.

field, which were used to compute the amount of unintentional bleaching. The rate of unintentional bleaching of the nearest-neighbors of the bleached nucleus was used to normalize the fluorescence recovery of the bleached nucleus (Fig. 9b).

Given the application to FRAP experiments, one challenge facing our nuclear segmentation and tracking algorithms is generating masks for the bleached nucleus, which often vanishes from both channels post-bleaching. To overcome this challenge, we used the relative positions of neighboring nuclei and assumed the bleached nucleus moved in a coordinated fashion with the surrounding nuclei and that it maintained its shape (Fig. 10a). As such, nucleus tracking also affects the segmentation of the bleached nucleus in the frames during which it has vanished. To test these assumptions, we conducted a comparative analysis between masks generated under normal conditions and those derived using the neighboring location-

based method, employing Intersection over Union (IoU) as our evaluation metric. The comparative results indicate that our approach yields an average IoU of .85 across more than 100 nuclei and 18 embryos, suggesting a high degree of accuracy (Fig. 10b-f). This performance metric further improves when the size of the nucleus remains consistent over the observed period.

Our work contributes an effective pipeline for segmenting and tracking nuclei, tailored specifically for biological data where such processes are inherently challenging yet fundamentally important. This pipeline proves especially valuable in contexts requiring accurate identification and continuous monitoring of nuclei to decipher cellular behaviors and interactions. The enhanced precision and efficiency in tracking provided by our pipeline offer substantial support to researchers engaged in examining complex biological environments. It facilitates

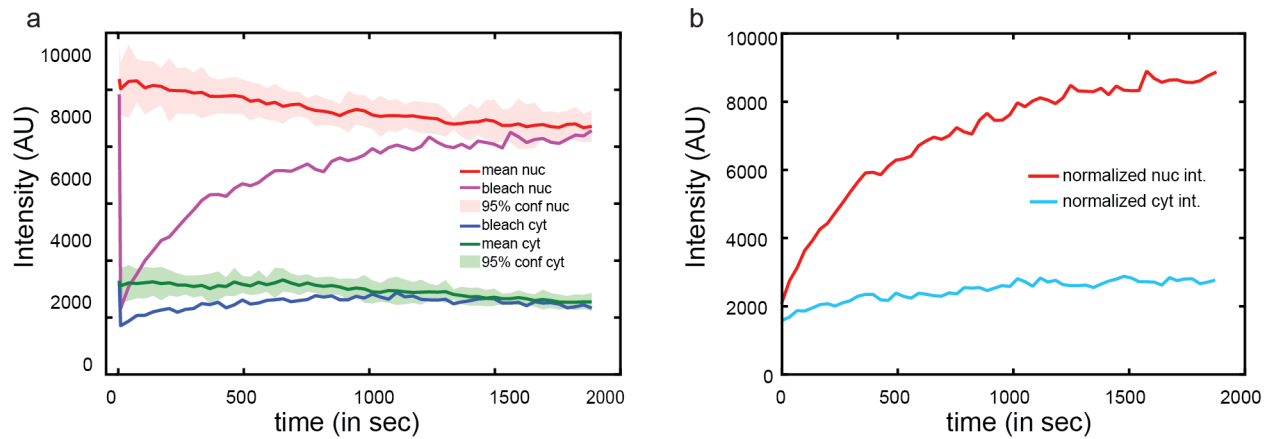


Fig. 9. Plots of intensities extracted from nuclear protein channel for nuclei and cytoplasmic compartments. (a) Intensities of bleached nucleus and cytoplasm and neighboring nuclei and cytoplasmic compartments. (b) Intensities of the bleached nucleus and cytoplasm normalized by the mean intensities of neighboring cytoplasm and nucleus, respectively.

a deeper understanding of nuclear dynamics, which is pivotal for advancing scientific knowledge in fields reliant on detailed cellular analysis.

The implications of our study extend beyond the immediate results, highlighting the transformative potential of our pipeline in changing the way researchers conduct segmentation and tracking of nuclei across diverse biological settings to extract quantitative measurements of biophysical parameters.

#### IV. CONCLUSION

Our study on FRAP experiments with blastoderm-stage *Drosophila* embryos has yielded a robust image analysis pipeline for nuclear segmentation and tracking, demonstrating high adaptability and accuracy across varying conditions. This pipeline, crucial for identifying fluorescence recovery in bleached nuclei, employs a points registration algorithm to ensure consistent nucleus identification over time. A notable contribution of our work is the innovative strategy developed to track nuclei that vanish post-bleaching. In instances where the bleached nucleus becomes invisible in both nuclear and protein channels, we utilized the positional data of adjacent nuclei to infer the location of the missing nucleus. This approach offers a reliable solution to a common challenge in fluorescence recovery experiments. By accurately tracing the bleached nucleus across frames where it is otherwise undetectable, our method enhances the fidelity of nuclear tracking and segmentation.

Looking forward, the potential for automating segmentation tasks using generated masks as training data opens up new avenues for research, promising to refine the application of our pipeline in biological studies.

#### REFERENCES

- [1] M. Mir, M. R. Stadler, S. A. Ortiz, C. E. Hannon, M. M. Harrison, X. Darzacq, and M. B. Eisen, "Dynamic multifactor hubs interact transiently with sites of active transcription in drosophila embryos," *Elife*, vol. 7, p. e40497, 2018.
- [2] W. J. de Jonge, H. P. Patel, J. V. Meeussen, and T. L. Lenstra, "Following the tracks: How transcription factor binding dynamics control transcription," *Biophysical journal*, vol. 121, no. 9, pp. 1583–1592, 2022.
- [3] A. Givré, A. Colman-Lerner, and S. Ponce Dawson, "Modulation of transcription factor dynamics allows versatile information transmission," *Scientific Reports*, vol. 13, no. 1, p. 2652, 2023.
- [4] F. Lu and T. Lionnet, "Transcription factor dynamics," *Cold Spring Harbor Perspectives in Biology*, vol. 13, no. 11, p. a040949, 2021.
- [5] T. Gregor, E. F. Wieschaus, A. P. McGregor, W. Bialek, and D. W. Tank, "Stability and nuclear dynamics of the bicoid morphogen gradient," *Cell*, vol. 130, no. 1, pp. 141–152, 2007.
- [6] N. M. Clark, E. Hinde, C. M. Winter, A. P. Fisher, G. Crosti, I. Blilou, E. Gratten, P. N. Benfey, and R. Sozzani, "Tracking transcription factor mobility and interaction in arabidopsis roots with fluorescence correlation spectroscopy," *Elife*, vol. 5, p. e14770, 2016.
- [7] S. N. Carrell, M. D. O'Connell, T. Jacobsen, A. E. Pomeroy, S. M. Hayes, and G. T. Reeves, "A facilitated diffusion mechanism establishes the drosophila dorsal gradient," *Development*, vol. 144, no. 23, pp. 4450–4461, 2017.
- [8] H. Al Asafen, N. M. Clark, T. Jacobsen, R. Sozzani, and G. T. Reeves, "Dorsal/nf- $\kappa$ b exhibits a dorsal-to-ventral mobility gradient in the drosophila embryo," *BioRxiv*, p. 320754, 2018.
- [9] A. E. Schloop, P. U. Bandodkar, and G. T. Reeves, "Formation, interpretation, and regulation of the drosophila dorsal/nf- $\kappa$ b gradient," *Current Topics in Developmental Biology*, vol. 137, pp. 143–191, 2020.
- [10] D. Axelrod, D. Koppel, J. Schlessinger, E. Elson, and W. W. Webb, "Mobility measurement by analysis of fluorescence photobleaching recovery kinetics," *Biophysical journal*, vol. 16, no. 9, pp. 1055–1069, 1976.
- [11] A. B. Houtsmuller, "Fluorescence recovery after photobleaching: application to nuclear proteins," *Microscopy Techniques*, pp. 177–199, 2005.
- [12] N. Lorén, J. Hagman, J. K. Jonasson, H. Deschout, D. Bernin, F. Cellaz-Zanacchi, A. Diaspro, J. G. McNally, M. Ameloot, N. Smisdom *et al.*, "Fluorescence recovery after photobleaching in material and life sciences: putting theory into practice," *Quarterly reviews of biophysics*, vol. 48, no. 3, pp. 323–387, 2015.
- [13] H. C. Ishikawa-Ankerhold, R. Ankerhold, and G. P. Drummen, "Advanced fluorescence microscopy techniques—frap, flip, flap, fret and flim," *Molecules*, vol. 17, no. 4, pp. 4047–4132, 2012.
- [14] B. L. Sprague and J. G. McNally, "Frap analysis of binding: proper and fitting," *Trends in cell biology*, vol. 15, no. 2, pp. 84–91, 2005.
- [15] F. Mueller, D. Mazza, T. J. Stasevich, and J. G. McNally, "Frap and kinetic modeling in the analysis of nuclear protein dynamics: what do we really know?" *Current opinion in cell biology*, vol. 22, no. 3, pp. 403–411, 2010.

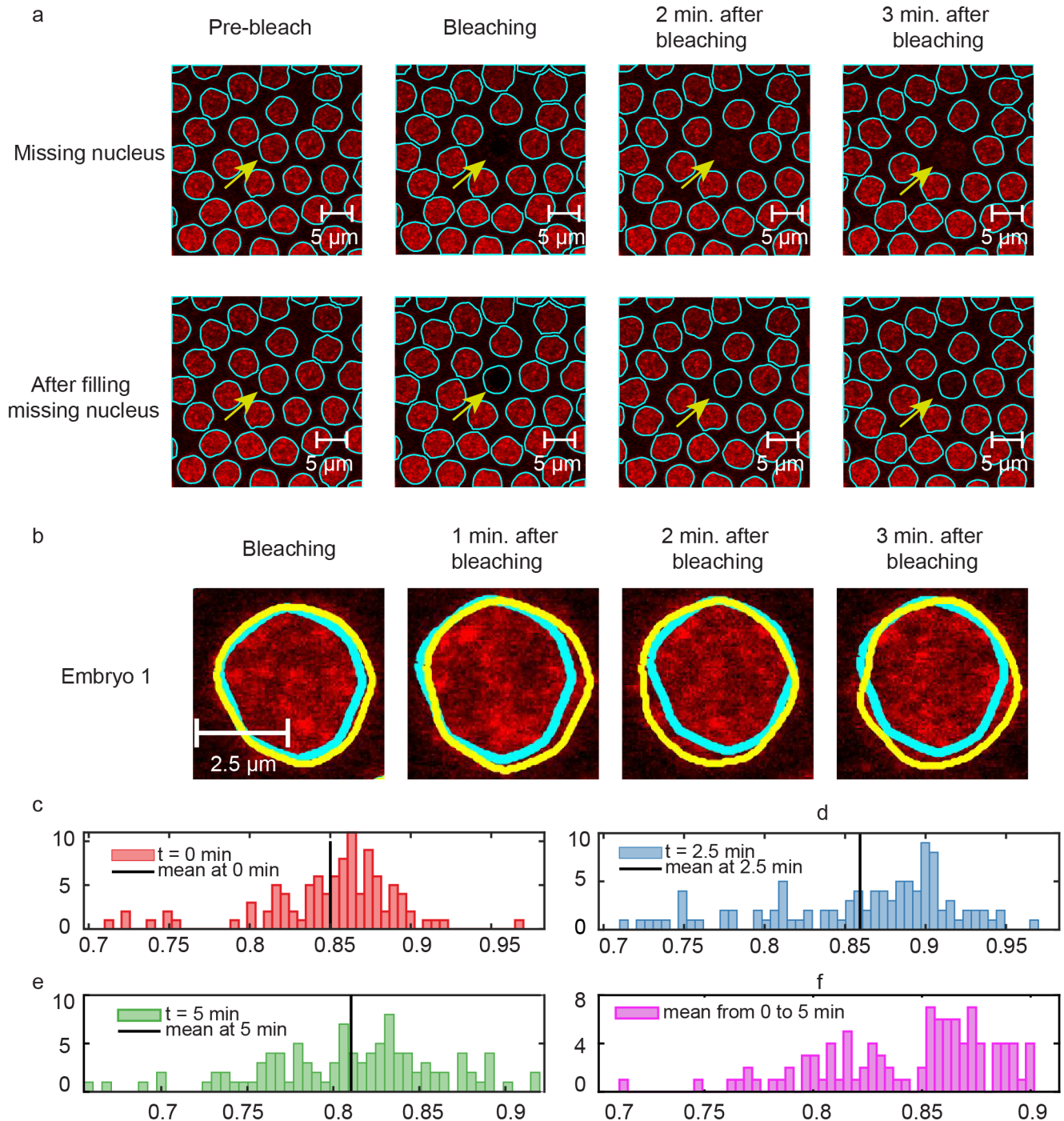


Fig. 10. (a) Results of image analysis when bleached nucleus goes missing. We use the initial mask of the bleached nucleus as a reference and move it through the frames using the centroid locations of neighbors to generate the projected location of the missing nucleus. (b) Comparisons of masks obtained via segmentation and the masks obtained via shifting the mask from the initial frame using the centroid locations of neighbors to generate the projected location. (c)-(f) Histograms of IOUs comparing the masks from segmentation and masks shifted using neighboring locations.

- [16] G. Carrero, D. McDonald, E. Crawford, G. de Vries, and M. J. Hendzel, "Using frap and mathematical modeling to determine the in vivo kinetics of nuclear proteins," *Methods*, vol. 29, no. 1, pp. 14–28, 2003.
- [17] H. Irshad, A. Veillard, L. Roux, and D. Racoceanu, "Methods for nuclei detection, segmentation, and classification in digital histopathology: a review—current status and future potential," *IEEE reviews in biomedical engineering*, vol. 7, pp. 97–114, 2013.
- [18] T. Hayakawa, V. Prasath, H. Kawanaka, B. J. Aronow, and S. Tsuruoka, "Computational nuclei segmentation methods in digital pathology: a survey," *Archives of Computational Methods in Engineering*, vol. 28, no. 1, pp. 1–13, 2021.
- [19] K. S. Beevi, M. S. Nair, and G. Bindu, "Detection of mitotic nuclei in breast histopathology images using localized acm and random kitchen sink based classifier," in *2016 38th annual international conference of the IEEE Engineering in Medicine and Biology Society (EMBC)*. IEEE, 2016, pp. 2435–2439.
- [20] T.-H. Song, V. Sanchez, H. EIDaly, and N. M. Rajpoot, "Dual-channel active contour model for megakaryocytic cell segmentation in bone

- marrow trephine histology images," *IEEE Transactions on Biomedical Engineering*, vol. 64, no. 12, pp. 2913–2923, 2017.
- [21] P. Shi, J. Zhong, R. Huang, and J. Lin, "Automated quantitative image analysis of hematoxylin-eosin staining slides in lymphoma based on hierarchical kmeans clustering," in *2016 8th International Conference on Information Technology in Medicine and Education (ITME)*. IEEE, 2016, pp. 99–104.
- [22] M. Neghina, C. Rasche, M. Ciuc, A. Sultana, and C. Tiganesteanu, "Automatic detection of cervical cells in pap-smear images using polar transform and k-means segmentation," in *2016 Sixth International Conference on Image Processing Theory, Tools and Applications (IPTA)*. IEEE, 2016, pp. 1–6.
- [23] Y. Al-Kofahi, W. Lassoued, W. Lee, and B. Roysam, "Improved automatic detection and segmentation of cell nuclei in histopathology images," *IEEE Transactions on Biomedical Engineering*, vol. 57, no. 4, pp. 841–852, 2009.
- [24] J. Qi, B. Wang, N. Pelaez, L. Rebay, R. W. Carthew, A. K. Katsaggelos, and L. N. Amaral, "Drosophila eye nuclei segmentation based on graph cut and convex shape prior," in *2013 IEEE International Conference on Image Processing*. IEEE, 2013, pp. 670–674.
- [25] F. Amat, W. Lemon, D. P. Mossing, K. McDole, Y. Wan, K. Branson, E. W. Myers, and P. J. Keller, "Fast, accurate reconstruction of cell lineages from large-scale fluorescence microscopy data," *Nature methods*, vol. 11, no. 9, pp. 951–958, 2014.
- [26] M. Veta, A. Huisman, M. A. Viergever, P. J. van Diest, and J. P. Pluim, "Marker-controlled watershed segmentation of nuclei in h&e stained breast cancer biopsy images," in *2011 IEEE international symposium on biomedical imaging: from nano to macro*. IEEE, 2011, pp. 618–621.
- [27] R. Ahasan, A. U. Ratul, and A. Bakibillah, "White blood cells nucleus segmentation from microscopic images of strained peripheral blood film during leukemia and normal condition," in *2016 5th International Conference on Informatics, Electronics and Vision (ICIEV)*. IEEE, 2016, pp. 361–366.
- [28] A. Bläßle, G. Soh, T. Braun, D. Mörsdorf, H. Preiß, B. M. Jordan, and P. Müller, "Quantitative diffusion measurements using the open-source software pyfrap," *Nature communications*, vol. 9, no. 1, pp. 1–14, 2018.
- [29] N. Emami, Z. Sedaie, and R. Ferdousi, "Computerized cell tracking: current methods, tools and challenges," *Visual Informatics*, vol. 5, no. 1, pp. 1–13, 2021.
- [30] D. M. Mount, N. S. Netanyahu, and J. Le Moigne, "Improved algorithms for robust point pattern matching and applications to image registration," in *Proceedings of the fourteenth annual symposium on Computational geometry*, 1998, pp. 155–164.
- [31] A. A. Goshtasby, *Image registration: Principles, tools and methods*. Springer Science & Business Media, 2012.
- [32] C. Yuan, X. Yu, and Z. Luo, "3d point cloud matching based on principal component analysis and iterative closest point algorithm," in *2016 International Conference on Audio, Language and Image Processing (ICALIP)*. IEEE, 2016, pp. 404–408.
- [33] N. Otsu, "A threshold selection method from gray-level histograms," *IEEE transactions on systems, man, and cybernetics*, vol. 9, no. 1, pp. 62–66, 1979.
- [34] Y. Chen and G. G. Medioni, "Object modelling by registration of multiple range images," *Image Vis. Comput.*, vol. 10, pp. 145–155, 1992.